This article has been accepted for publication in a future issue of this journal, but has not been fully edited. Content may change prior to final publication. Citation information: DOI 10.1109/TPWRD.2019.2931838, IEEE Transactions on Power Delivery

Replicating Real-World Wind Farm SSR Events

Yin Li, *Student Member, IEEE*, Lingling Fan, *Senior Member, IEEE*, Zhixin Miao, *Senior Member, IEEE*

***Abstract*—In 2017, three sub-synchronous resonance (SSR) events were reported in the transmission system of Electric Reliability Council of Texas (ERCOT). These three events with different consequences are due to the same cause, i.e., Type-3 wind farms radially connected to a series compensated transmission line. The objectives of this paper are (i) to build a testbed to replicate these real-world events and investigate what causes the different consequences, (ii) to find out the impact of wind penetration level and wind speed on SSR, and (iii) to investigate how to mitigate SSR. The replication testbed is built in MATLAB/Simpowersystems with each wind farm represented by a single aggregated wind turbine with full dynamics. The challenge of replication is the limited information about those three events, the ERCOT system, and the wind farms. Nevertheless, relying on simplification and assumptions, we are able to replicate the three events. Our contributions include the configured testbed for Type-3 wind farm SSR studies, diagnosis of impacting factors on SSR, and the confirmation of an SSR mitigation strategy through grid-side converter ac voltage command signal modulation.**

***Index Terms*—Sub-synchronous resonance, DFIG-based wind farm, modeling and control.**

I. Introduction

MORE and more wind farms are built in recent years and they are usually located in remote areas and rely on long distance transmission for power delivery. Series compensation are commonly used in long-distance transmission lines to reduce electricity distance and increase transfer capacity. On the other hand, subsynchronous resonance (SSR) is a challenging issue in type-3 wind farms connected to the series compensated networks [1]–[3].

From August 2017 to October 2017, three SSR events were recorded by Electric Reliability Council of Texas (ERCOT) [4]. These three events happened in the same transmission system as shown in Fig. 1. The voltage level of main transmission lines is 345 kV. Six wind plants are integrated at three stations: Cenizo, Del Sol, and Pomelo. The series compensation line is employed to connect Cenizo station and Del Sol station. Two end stations, San Miguel and N Edinburg, are connected to the main grid. The voltage and current of each event were recorded and presented in [4].

All of three SSR events were caused by Type-3 wind farms radially connected to the series compensated transmission line after transmission line outages.

- Event 1: On August 24th, Del Sol - Pomelo line was tripped. This line outage left Plants 3 & 4 being radially connected to the Cenizo-Del Sol series compensated line. 25.6 Hz SSR was observed in instantaneous currents in abc-frame until Plants 3 and 4 were tripped by the protection devices. The currents and the corresponding frequency spectrum are shown in Fig. 10a.
- Event 2: On September 27th, Lobo - Cenizo line was tripped. This line outage left Plants 1 & 2 being radially connected to the Cenizo-Del Sol series compensated line. 22.5 Hz SSR was observed which led to the tripping of wind plants 1 & 2. The currents and the corresponding frequency spectrum are shown in Fig. 10b.
- Event 3: On October 27th, Del Sol - Pomelo line was tripped. 26.5 Hz SSR was observed. This event did not trigger the protection device and Plants 3 &4 were not tripped. The currents and the corresponding frequency spectrum are shown in Fig. 10c.

Y. Li, L. Fan and Z. Miao are with Dept. of Electrical Engineering, University of South Florida, Tampa FL 33620. Email: linglingfan@usf.edu.

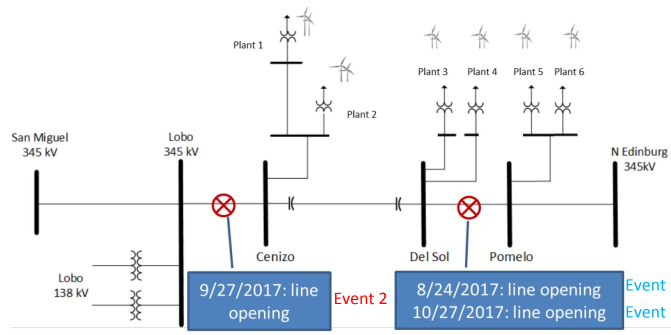

Fig. 1: System topology [4].

It is understandable that for Event 1 and Event 2, the resulting systems have different equivalent compensation levels and hence there is difference in SSR frequency. On the other hand, it is puzzling to see Event 1 and Event 3, with the same line tripped, led to one case that SSR is severe enough being detected by the protection device and the other case that is less severe. We also noticed that in Event 3, more wind power was generated compared to that in Event 1. Yet the system is more stable in Event 3 compared to that in Event 1.

The immediate and *first* objective of this paper is to build an electromagnetic transient (EMT) testbed, replicate these real-world events, and understand what causes the different consequences. The *second* objective is to predict the system's SSR stability with higher wind penetration. Influence of wind speeds on SSR stability will also be examined. Finally, the *third* objective is to investigate how to mitigate SSR. In the authors' 2012 research paper [5], an SSR mitigation strategy was proposed and tested in an analytical model with simplification, e.g., phase-locked-loop (PLL) dynamics ignored. With this real-world replication testbed ready, this strategy can be further confirmed.

a) Literature Survey: Real-world type-3 wind farm SSR events in Texas have been studied in many papers since 2012, e.g., [3], [6]–[11]. In all the cited papers, detailed parameters of the testbeds are not given, which result in testbeds not

This article has been accepted for publication in a future issue of this journal, but has not been fully edited. Content may change prior to final publication. Citation information: DOI 10.1109/TPWRD.2019.2931838, IEEE Transactions on Power Delivery

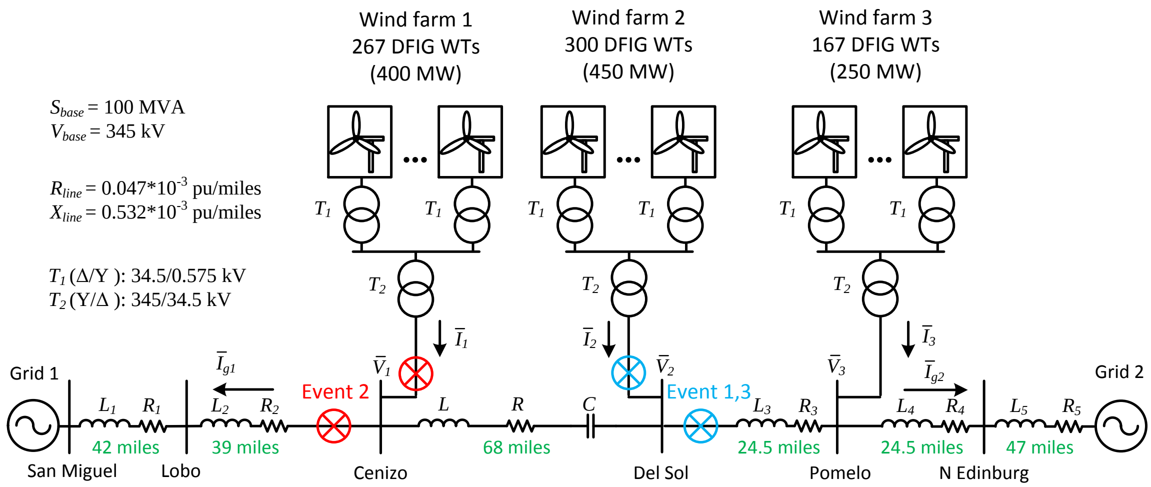

Fig. 2: Simpowersystems testbed.

replicable. Meanwhile, none of those testbeds focuses on the south region of Texas studied in this paper. The Texas transmission system keeps evolving. We have used most recent public information to have many new transmission projects considered.

A survey of [3], [6]–[11] is as follows. To analyze type-3 wind farm SSR events in Texas using frequency scanning, authors of [6] built two PSCAD/EMTDC testbeds for the Silverton substation and Rio Hondo substation respectively. On the other hand, detailed parameters of the test systems are not given. [7] investigated type-3 wind farm SSR by comparing the real records and EMT simulation results. The testbed was designed based on a simple and non-proprietary system. [3], [8]–[10] presented EMT simulation results to investigate type-3 wind farm SSR phenomena. The papers indicate that the testbeds are built based on the particular sections of the Texas grid. Though the topologies of the test systems are presented, detailed parameters, e.g., line impedance and parameters of wind turbines, are not given. Finally, [11] uses the relevant portion of the Texas grid model to test the reactance scan and the paper presents the impedance of transmission lines and transformers. Parameters relevant to wind farms are not presented. In addition, the testbed focuses a different portion of the Texas transmission system.

b) Challenges: The testbed will be built in MATLAB/Simpowersystems. It is not possible nor necessary to model an entire ERCOT transmission grid to replicate these three events. The *foremost* challenge is to come up with a simplified yet adequate system topology. Here the focus is the San Miguel to N. Edinburg transmission system and the six wind plants located at Cenizo, Del Sol, and Pomelo. Hence, we make the main assumption of the testbed topology to treat the rest ERCOT system as one voltage source behind San Miguel 345 kV substation and another behind N. Ediburg 345 kV substation.

The *second* challenge is that the information about these events and the transmission system is very limited. None of the system information, e.g., line lengths, compensation level, wind plant parameters such as size, number of wind turbines, is available in [4]. To configure the testbed, we rely on public information only. Based on the public transmission project information, length of transmission lines, compensation level, and the names of wind farms can be determined. Typical 345 kV transmission line per unit length resistance and reactance are used. With the names of wind farms identified, we further found the type of wind turbines and the capacity of the wind farms also through public information.

Nonetheless, detailed information of wind turbines, e.g., converter control structure, control parameter, are confidential to wind manufacturers. For this part, we adopt the 1.5 MW doubly-fed induction generator (DFIG) example in MATLAB/Simpowersystems as the building block. Detailed rotor-side converter structure and grid-side converter structure can be found from MATLAB/Simpowersystems demo *Wind Farm - DFIG Average Model*.

Two other important parameters are unknown: the number of online wind turbines and the wind speed. Their values need to be fine tuned because their effect on system stability is significant. Hence, sensitivity analysis is conducted to examine the effect of number of online wind turbine and wind speed's influence on SSR.

Based on the sensitivity analysis, the testbed is tuned to match the simulation results with the data records presented in [4]. We also identified that wind speed at Event 3 is higher compared to that at Event 1. The system is more stable at Event 3 compared to that at Event 1 due to higher wind speed. This observation aligns with the remarks made in [1] through analysis.

Finally, SSR mitigation is investigated using the testbed. There are two types of existing methods. The first type is using additional FACTS devices [12], [13]. The second type is to add control loops on top of rotor-side converter (RSC) and/or grid-side converter (GSC) controllers, e.g., [5], [14]. The second type method can be implemented with less cost.

SSR control was proposed in the authors' prior work [5] for Type-3 wind using supplementary control of GSC. Compared with many other SSR mitigation strategies proposed after [5], e.g., [14], the control in [5] is a simple feedback control strategy with a single input (series capacitor voltage) and single output (supplementary signal to GSC's ac voltage command).

This article has been accepted for publication in a future issue of this journal, but has not been fully edited. Content may change prior to final publication. Citation information: DOI 10.1109/TPWRD.2019.2931838, IEEE Transactions on Power Delivery

On the other hand, strategy in [14] requires multiple inputs and multiple outputs. Simple single-input single-output (SISO) control is preferred. The tests conducted in this paper give further validation of the SISO control.

The work on SSR mitigation in the paper extends the prior work in [5]. Control implementation details and control block design details, including capacitor voltage estimation using local signals and high-pass filter implementation, are investigated. The details of the improvement is presented in Section V. Moreover, in [5], the supplementary control was tested on an analytical model based on dq-frames with simplification (e.g. PLL ignored). In this paper, the supplementary control is tested in a practical EMT testbed with full dynamics.

c) Organization: The rest of the paper is organized as follows. Section II presents the testbed topology and the parameter setting procedure based on known information. In Section III, sensitivity analysis of online wind turbine number and wind speed is conducted. Based on the analysis, Section IV explains how these two factors are tuned to match the real-world data records. The replication results are compared with the data records. In Section V, the supplementary SSR control is implemented and its performance on SSR mitigation is examined. Section VI concludes the paper.

II. Testbed parameter configuration

A. Transmission line parameters

The testbed is built in MATLAB/Simpowersystems and its topology is shown in Fig. 2. The testbed has six 345 kV stations and three of them are interconnected with the wind farms. Two end stations of this transmission system are San Miguel and N Eidinburg which are connected to the main grids represented by infinite buses.

Transmission line information was collected based on the public project reports from Electric Transmission Texas (EET). According to the report of Rio Grande Valley projects [15], the transmission line is 156 miles from ETT's Lobo station to AEP's North Edinburg station. The report of Lower Rio Grande Valley Projects [16] provides the map of this transmission line shown in Fig. 5. Based on the map, the lengths between two stations are stimated. The length from Lobo station to Cenizo station is around 39 miles while the length from Del Sol station to N Edinburg station is 49 miles. The length from Cenizo station to Del Sol station is 68 miles. Because the portions between Del Sol station and N Edinburg are not provided, it is assumed that Pomelo station is at the middle point ($L_3 = L_4$). The additional line from San Miguel station to Lobo station is found to be 42 miles and it is not shown in Fig. 5. The power base is 100 MVA and the voltage base is 345 kV. The per-unit values of line impedance are calculated based on the transmission line parameters used in MATLAB/Simpowersystems Wind Farm-DFIG Average Model. The per unit length resistance and reactance are 0.047×10^{-3} pu/mile and 0.532×10^{-3} pu/mile.

B. Compensation level

The total reactance of two series capacitors is 48 Ω and they are installed between Cenizo and Del sol stations [15]. The compensation level of this line (Lobo to N Edinburg) is around 49%.

R_5 and L_5 are determined by trial and error of Event 2 simulation to match the ratio of the SSR component at 22.5 Hz versus the fundamental component at 60 Hz ($\frac{320\text{A}}{230\text{A}}$).

The per-unit values and real values for the transmission system are summarized in Table I including the transmission lines and the transformers. Notice: X_{T1} and R_{T1} indicate the total impedance of T_1 for each whole wind farm.

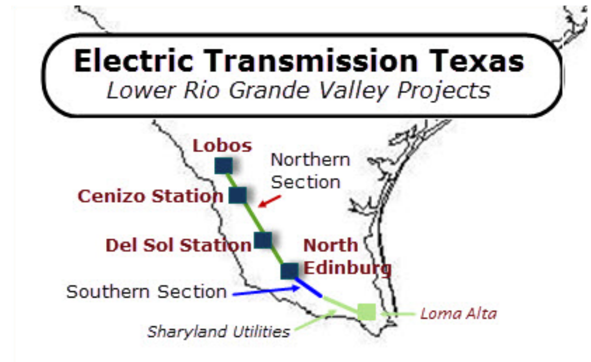

Fig. 5: The map of Lower Rio Grade Valley projects [16].

TABLE I: Parameters of transmission system

Parameter	Value (SI)	Per-unit (pu)
S_{base}	100 MW	
V_{base}	34.5 kV	
$L_{T1}(X_{T1}), R_{T1}$	31.6 μH, 1.2 mΩ	0.002, 0.0002
V_{base}	345 kV	
$L_{T2}(X_{T2}), R_{T2}$	3.16 mH, 0.12 Ω	0.002, 0.0002
$L(X_L), R, C(X_C)$	114 mH, 4.76 Ω, 55 μF	0.0362, 0.004, 0.041
$L_1(X_1), R_1$	69 mH, 2.26 Ω	0.022, 0.0019
$L_2(X_2), R_2$	66 mH, 2.26 Ω	0.021, 0.0019
$L_3(X_3), R_3$	41 mH, 1.43 Ω	0.013, 0.0012
$L_4(X_4), R_4$	41 mH, 1.43 Ω	0.013, 0.0012
$L_5(X_5), R_5$	79 mH, 2.63 Ω	0.025, 0.0022

C. Wind farm parameters

The name of each wind plant can be found from the public project reports of utilities. The public wind power database also gives detailed information about each wind plant, including capacity, the number of wind turbines, and types.

According to [16], two wind plants, Javelina I and II, are interconnected to Cenizo station and their total capacity is 450 MW. Two wind plants, Los Vientos III and IV, are interconnected to Del Sol station and their total capacity is 400 MW. According to [17], wind plants Los Mirasoles are interconnected to Pomelo station and their total capacity is 250 MW. In all of six wind plants, the type of wind turbine is Type-3 DFIG and their rated wind speeds are around $11 \sim 12$ m/s.

In the testbed, the wind plants integrated at the same bus are aggregated as one DFIG wind farm. Each wind farm is represented by one DFIG wind turbine module from MATLAB demo, *Wind Farm - DFIG Average Model*. This demo is built based on the GE 1.5 MW wind turbine-generators. Dynamic modeling of this DFIG was reported in [18]. The demo uses the realistic control systems, control parameters, and machine

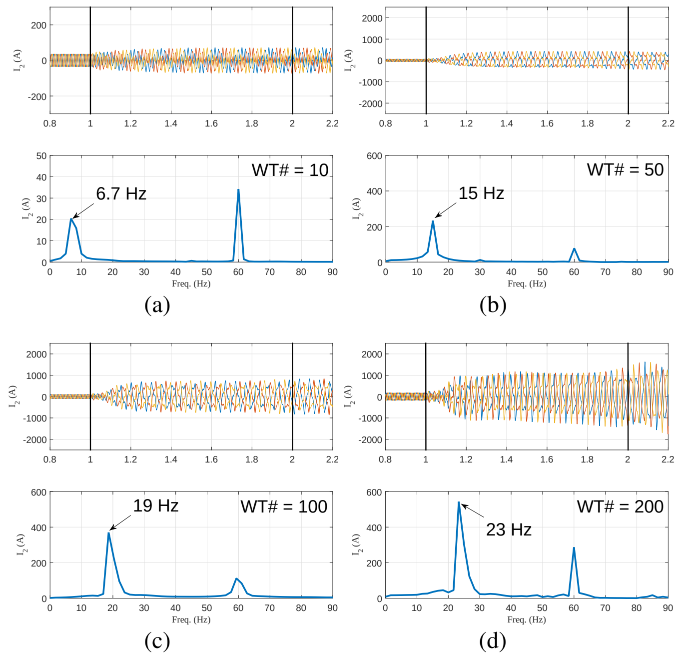

Fig. 3: Effect of # of online wind turbines in WF2. (3a) 10 wind turbines; (3b) 50 wind turbines; (3c) 100 wind turbines; (3d) 200 wind turbines.

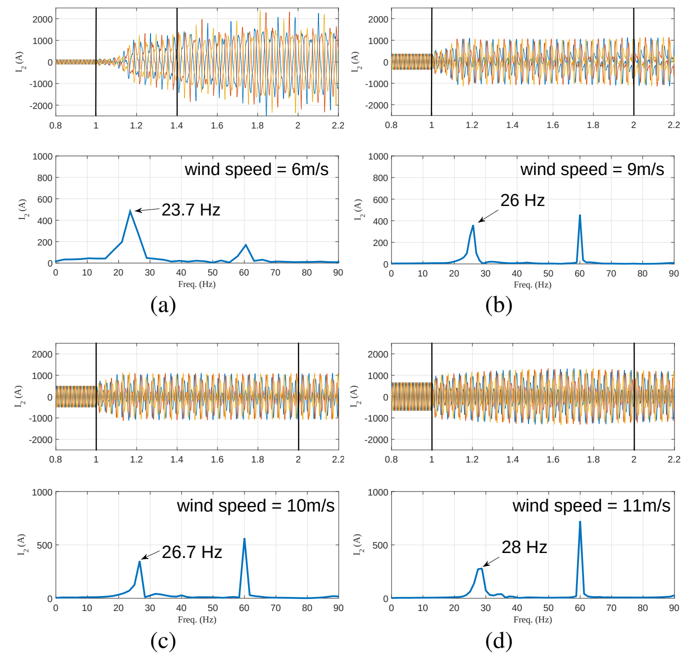

Fig. 4: Effect of wind speed. (4a) 6 m/s; (4b) 8 m/s; (4c) 10 m/s; (4d) 11 m/s (rated).

parameters. The parameters of the wind turbine are listed in Table III in Appendix. In testbed building, we assume that each wind turbine is 1.5 MW. Hence the total numbers of wind turbines at the three wind farms are computed to be 267, 300, and 167 respectively.

III. Sensitivity Analysis

The parameters of transmission lines and wind farm capacities can be found in public domain, information of number of online wind turbines and wind speed during each event can only be guessed. On the other hand, the two factors (online wind turbines and wind speed) have significant impact on SSR stability. In this section, sensitivity analysis is conducted to examine the influence of these two factors. The sensitivity of each factor is analyzed. Event 1 (Del Sol to Pomelo line tripping) is considered for the testbed simulation. Parameters of Event 1 are used and they were listed in Table I and Table II. Based on the sensitivity analysis, the number of online wind turbines and wind speed will be fine tuned for each of SSR event in next section.

A. Number of Online Wind Turbines

Due to the line tripping, WF2 is radially connected to the RLC circuit and SSR occurs. In sensitivity analysis, the number of online wind turbines of WF2 is varied from 10 to 300 to create various scenarios. The wind speed is kept as 7.5 m/s. The simulation results for four scenarios are presented in Fig. 3. When 10 wind turbines is online, the magnitude of SSR is smaller than that of the nominal component. However, the SSR magnitude is three times larger than that of the nominal component when 50 or 100 wind turbines were online. This study shows that with more online wind turbines, the system becomes less stable.

Fig. 6a lists the corresponding SSR frequencies under seven scenarios. It is found that the SSR frequency varies from 6.7 Hz to 26 Hz. More online wind turbines will lead to increase in the frequency of SSR and an less stable system.

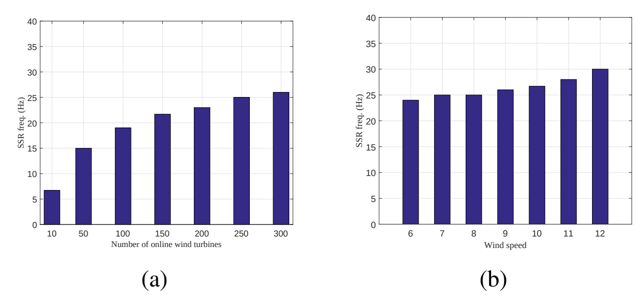

Fig. 6: Effect of wind turbine number and wind speed on SSR frequency. (6a) number of online wind turbines; (6b) wind speed.

For Event 1, WF2 is radially connected to the RLC circuit. An analytical model is built in MATLAB/Simulink to represent WF2 radially connected to an equivalent RLC circuit. Fig. 7 presents the eigenvalue loci with the number of wind turbines varying. Fig. 7b shows that the oscillation frequency is reduced from 53.5 to 34 Hz in dq frame when the number of online wind turbines is increased from 10 to 300. This indicates that the oscillation frequency increases from 6.5 Hz to 26 Hz in abc frame. The eigenvalue analysis results corroborate with the EMT testbed simulation results.

B. Wind Speed

Wind speed affects the power penetrated into the grids. Higher wind speed corresponds to more wind power injection

This article has been accepted for publication in a future issue of this journal, but has not been fully edited. Content may change prior to final publication. Citation information: DOI 10.1109/TPWRD.2019.2931838, IEEE Transactions on Power Delivery

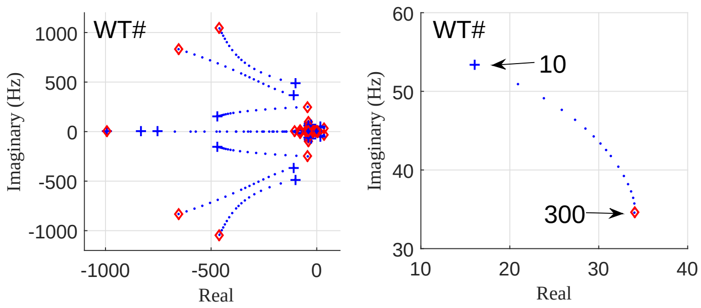

(a) (b)

Fig. 7: Eigenvalue loci with the number of online wind turbines varying from 10 to 300. (7a) The entire eigenvalue loci. (7b) Zoom-in section of the dominate eigenvalues.

into the grid. On the other hand, higher wind speed means better SSR stability, a fact indicated based on small-signal analysis in [1] and observed in real world North China Type-3 wind farms [2]. In this sensitivity analysis, wind speed is varied from 6 m/s to 12 m/s for all of three wind farms.

The simulation results were summarized in Fig. 4. FFT plots in Fig. 4 shows that the nominal component becomes larger and the SSR component becomes smaller with wind speed increasing. The dynamic responses of the current confirm that higher wind speed leads to better SSR stability. We use this fact to project that the different consequences of Event 1 and Event 3 are mainly due to different wind speed.

Fig. 6b presents the SSR frequencies under different wind speed conditions. The frequency of SSR increases from 23.7 Hz to 30 Hz with wind speed increasing.

Fig. 8 shows the eigenvalue loci with the wind speed changing from 6 m/s to 12 m/s. The dominant eigenvalue loci in Fig. 8b indicate that the oscillation frequency in the dq frame is changed from 37 Hz to 30 Hz. This indicates that the SSR frequency is in the range of 23 to 30 Hz in the abc-frame. Therefore, the eigenvalue loci is validated by the bar plot in Fig. 6b.

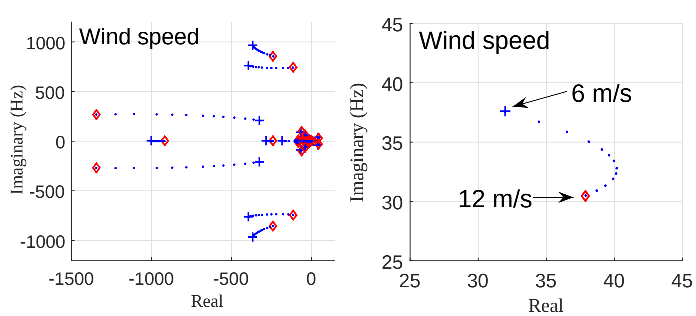

(a) (b)

Fig. 8: Eigenvalue loci with the wind speed changing from 6 m/s to 12 m/s. (8a) The entire eigenvalue loci; (8b) zoom-in of the dominant eigenvalues.

IV. Replication by fine tuning

One challenge of replication is a lot of information is unknown. For example, how many wind turbines online at each event is unknown. The wind speed at each event is also unknown. On the other hand, both factors affect the generated wind power and SSR stability.

[4] presents the real-world event recorded data shown in Fig. 10. The instantaneous current plots at 345 kV level are available. Yet no information is provided to indicate at which locations the currents were measured. We noted that the currents became zero after WF2 tripped in Event 1 while they had values in Event 2 after WF1 was tripped. In Event 1 and Event 3, WF2 were radially connected to the RLC circuit. If the measured current is the current through the RLC line, then the current exported from WF2, I_2, is the same as the measured current in Event 1 and Event 3. In Event 2, Lobo to Cenizo line was tripped and WF1 was initially radially connected to Grid 2 through the RLC circuit and then tripped. Since the current record shows nonzero values after WF1 was tripped, the measured current should not come from the RLC line. On the other hand, if we assume that the current measurement is from from Del Sol to Pomelo, the current flow should be the combination of WF1 and WF2 after the line tripping. The FFT record in [4] shows 300 A for the 60 Hz component magnitude, a comparable amount of WF2's output in Event 1. This amount appears low as the combination of WF1 and WF2 outputs. Thus, we make assumption that the currents recorded are all WF2's output.

The number of online wind turbines and wind speed are then estimated for each event using the FFT analysis results in Fig. 10 of the recorded data. It is assumed that the wind speed is the same for all wind farms for each event. The estimated values for each event are listed in Table II. Detailed tuning procedure is given as follows.

TABLE II: Parameters of wind farms (1.5 MW each turbine)

	Capacity (MW)	Total	Event 1	Event 2	Event 3
WF1 (#WTs)	400	267	267	110	200
WF2 (#WTs)	450	300	250	220	200
WF3 (#WTs)	250	167	167	167	167
Wind Speed (m/s)		11	7.5	7.9	10.5

In Event 1, WF2 is radially connected to the RLC circuit. Note that the total number of the wind turbines of WF2 is 300. We conducted experiments and found that SSR frequency has less to do with wind speed but more to do with the number of online wind turbines. Based on Event 1's SSR frequency (25.6 Hz), the number of online turbines of WF2 is tuned to be 250 through trial and error. Then the wind speed is tuned to be 7.5 m/s so that the magnitudes of the SSR component and the fundamental component can match the recorded data.

The same line was tripped in Event 1 and Event 3, which left WF2 radially connected to the RLC circuit. While the 60 Hz component of WF2 current is 340 A in Event 1, this number is 430 A in Event 3 according to the recorded data shown in Fig. 10. The increase in WF2 current is possibly due to the increase in wind speed or the number of wind turbines online. However, the system was more stable in Event 3. Small-signal analysis in [5] indicates that higher wind speed leads to a more stable system while small-signal analysis in [19] indicates that more online wind turbines leads to a less stable system. Hence, we reasoned that the increase in WF2

This article has been accepted for publication in a future issue of this journal, but has not been fully edited. Content may change prior to final publication. Citation information: DOI 10.1109/TPWRD.2019.2931838, IEEE Transactions on Power Delivery

current is due to wind speed increase rather than online wind turbine number increase. Once the wind speed is increased to be 10.5 m/s, the 60 Hz component's magnitude becomes much higher than 430 A while the SSR component's magnitude becomes less than 350 A (recorded data). We then reduce the number of online wind turbines in WF2 from 250 to 200 to match the 60 Hz component magnitude. This reduction also causes the SSR component magnitude getting further reduced. On the other hand, WF1 is not radially connected the RLC circuit. Increasing the power from WF1 will make the overall system more stable while decreasing the power from WF1 will make the overall system less stable. By reducing the number of wind turbines in WF1 from 267 to 200, the SSR component magnitude gets slightly increased to match 340 A.

In Event 2, the WF1 is radially connected to the RLC circuit and the SSR frequency is 22.5 Hz. Our experiments indicate that the number of online wind turbines influences the SSR frequency. More turbines lead to higher SSR frequency. If we assume all 267 turbines are online, the SSR frequency is 25 Hz. Reducing the number to 110 leads to 22.5 Hz SSR component. Further, wind speed is tuned to be 7.9 m/s to match the SSR component magnitude (320 A). As the final step, since the measured current is WF2 current and to match the 60 Hz fundamental component current at 230 A, the number of online turbines in WF2 is tuned to be 220.

Fig. 9 shows the flowchart on how to get similar SSR frequency and amplitude. $\hat{I}_{SSR}$ and $\hat{I}_0$ notate the amplitudes of SSR and fundamental components respectively.

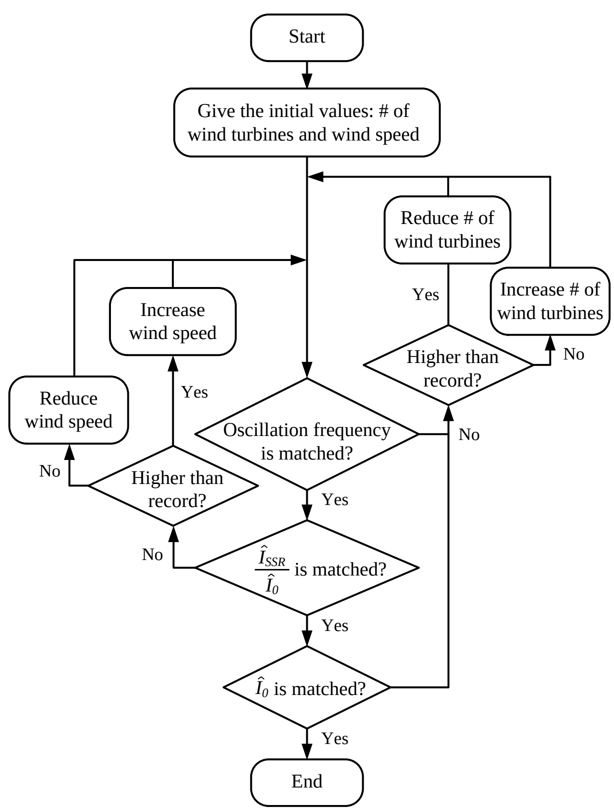

Fig. 9: Flowchart of testbed parameter tuning.

A. Replication results

The replication results are produced using the same sequence of tripping operations in the real-world events. The transmission line was tripped at 1s for all three events. In Event 1, at 2 seconds, WF2 tripped. In Event 2, at 2 seconds, WF1 tripped. Fig. 11 presents the replication results including WF2 currents and FFT spectrum of the WF2 currents. It can be seen that our replication results have very similar frequencies and magnitudes of the SSR and fundamental components with those from the recorded data.

Moreover, the replication explains why Event 1 and Event 3 lead to different outcomes. Wind speed plays an important role in SSR stability.

Remarks: It shall be noted that the testbed and simulation results from this paper may contain uncertainty. Operating conditions at different events may deviate from those of the real-world scenarios. A possible solution is to have more field measurements available and conduct refined tuning to make results closer to the real-world.

V. SSR Mitigation

The improved SSR supplementary control on top of GSC control is implemented in the testbed to mitigate the SSR. Fig. 12 shows the structure of a Type-3 wind turbine connected to a series compensated line.

Vector control is usually employed in the GSC which controls the DC-link voltage ($V_{\rm dc}$) and the PCC voltage ($V_{\rm pcc}$). The supplementary SSR control modulates the PCC voltage command. Analysis in [5] indicates that the voltage over the series capacitor ΔV_c is the best input signal for pure proportional control compared to other signals such as machine speed and line current ΔI_c. The modulation signal ΔV_{SSR} is generated after amplifying the input signal through a proportional gain K_{Vc}.

This input signal ΔV_c is a remote signal for wind farm GSC. Communication links need to be established for this SSR control. To avoid the cost of this infrastructure, [5] suggested to obtain ΔV_c using local measurements, i.e., the wind farm current. This strategy is implemented in this paper. When a wind farm is radially connected to the series compensated line, the wind farm current is approximately same as the instantaneous currents through the series compensated line $i_{c,abc}$. The capacitor voltages $v_{c,abc}$ can be estimated by integrating the instantaneous currents. (1) gives the relationship between the three-phase voltages and currents in abc-frame.

$$C\frac{dv_{c,abc}}{dt} = i_{c,abc}, \;\; v_{c,abc} = \frac{1}{C}\int i_{c,abc} \qquad (1)$$

The improved SSR control scheme is shown in Fig. 13. The instantaneous three-phase currents at 575 V level are measured and sent to integrators. The obtained signals then pass a high-pass filter ($\frac{0.1s}{1+0.1s}$) to get rid of dc component. The signals are amplified with a gain $K_1 = 1.0757 \times 10^{-4}$ to have per unit values. The three-phase signals now emulate $v_{c,abc}$. Its magnitude V_c is computed after abc to dq transformation. To have only the fast dynamics considered, another HPF is used before passing V_c to K_{Vc} unit to generate the modulation

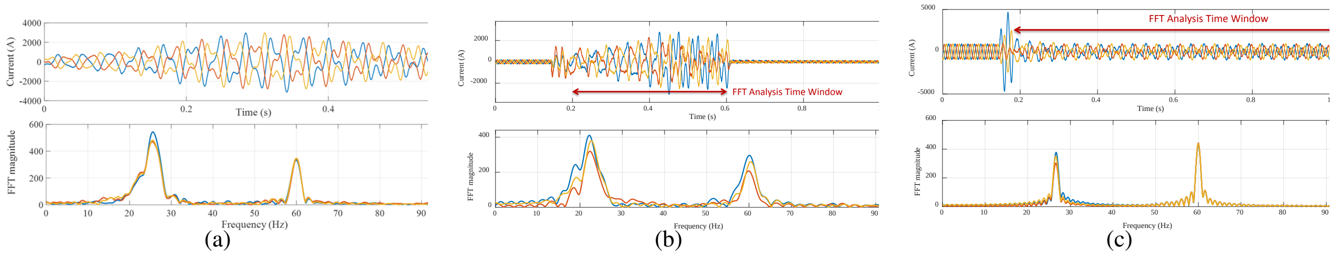

Fig. 10: Recorded real-world data. Event 1 (11a): 25.6 Hz. Event 2 (11b): 22.5 Hz. Event 3 (11c): 26.5 Hz.

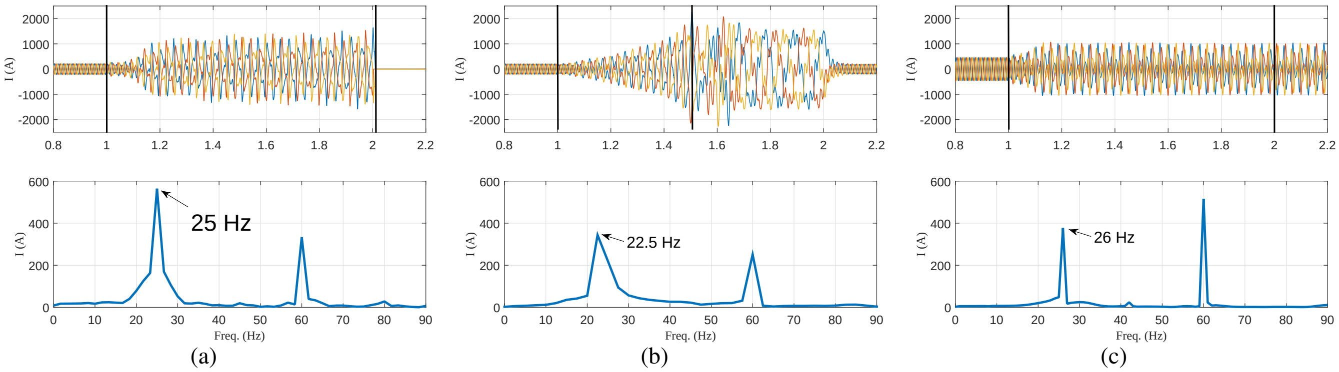

Fig. 11: Simulation results based on the testbed. Event 1 (11a); Event 2 (11b); Event 3 (11c).

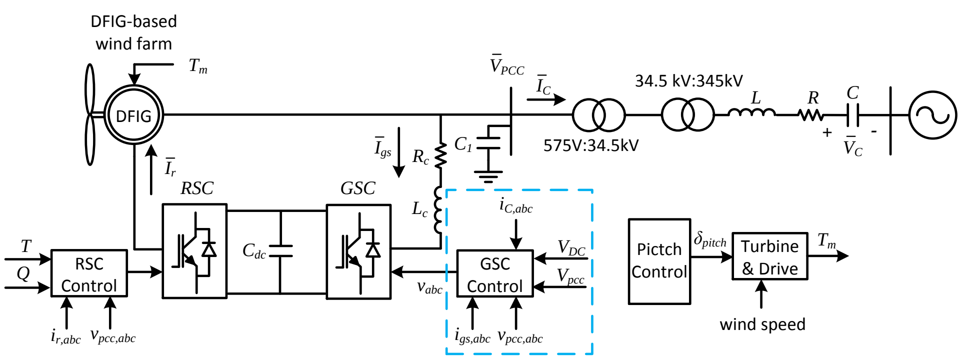

Fig. 12: Topology of Type-3 wind connected to the series compensated line.

signal ΔV_{SSR}. Compared with the supplementary control proposed in [5], the improved one has two more components, the high-pass filter (HPF) and K_1.

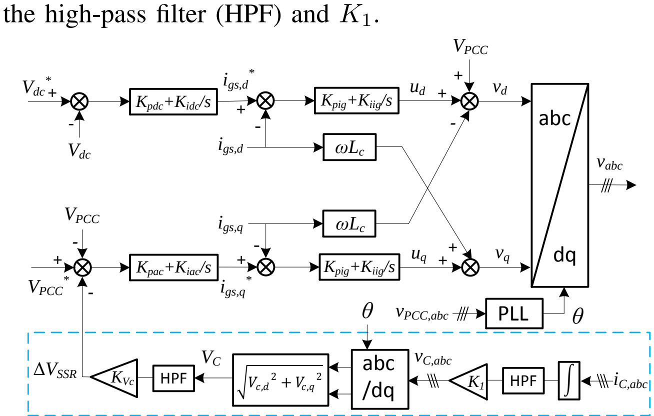

Fig. 13: SSR control scheme in the GSC control loop.

Event 1 (Del Sol - Pomelo line tripping) is used to test the performance of the SSR control. The line from Del Sol to Pomelo was open at 1 second which leaves WF2 being radially connected to the RLC circuit. WF2 is equipped with the SSR mitigation control. The simulation results are presented in Fig. 14, including the three-phase currents in Ampere at 345 kV level, the three-phase voltages in kV at 345 kV level, FFT of the current, power from from WF2 in pu, PCC voltage in pu, V_c signal of the SSR control, and the SSR modulation signal ΔV_{SSR}. The left column shows the dynamic responses of the system without the SSR control while the right column presents the system with the SSR control.

Without the SSR control (by setting $K_{Vc} = 0$), the SSR aggravates over time. The oscillation is approximately 25 Hz and has a much larger magnitude compared to that of the 60 Hz component. After applying the SSR control ($K_{Vc} = 0.8$), the system is stable after the line tripping. Fig. 14b shows that the SSR is well damped and FFT cannot detect the SSR component. Fig. 14d shows that the system became stable after a short transient period of about 0.1 seconds. The modulation signal is within the limit of ± 0.05 pu. This case study demonstrates the effectiveness of the SSR mitigation scheme proposed in [5].

This article has been accepted for publication in a future issue of this journal, but has not been fully edited. Content may change prior to final publication. Citation information: DOI 10.1109/TPWRD.2019.2931838, IEEE Transactions on Power Delivery

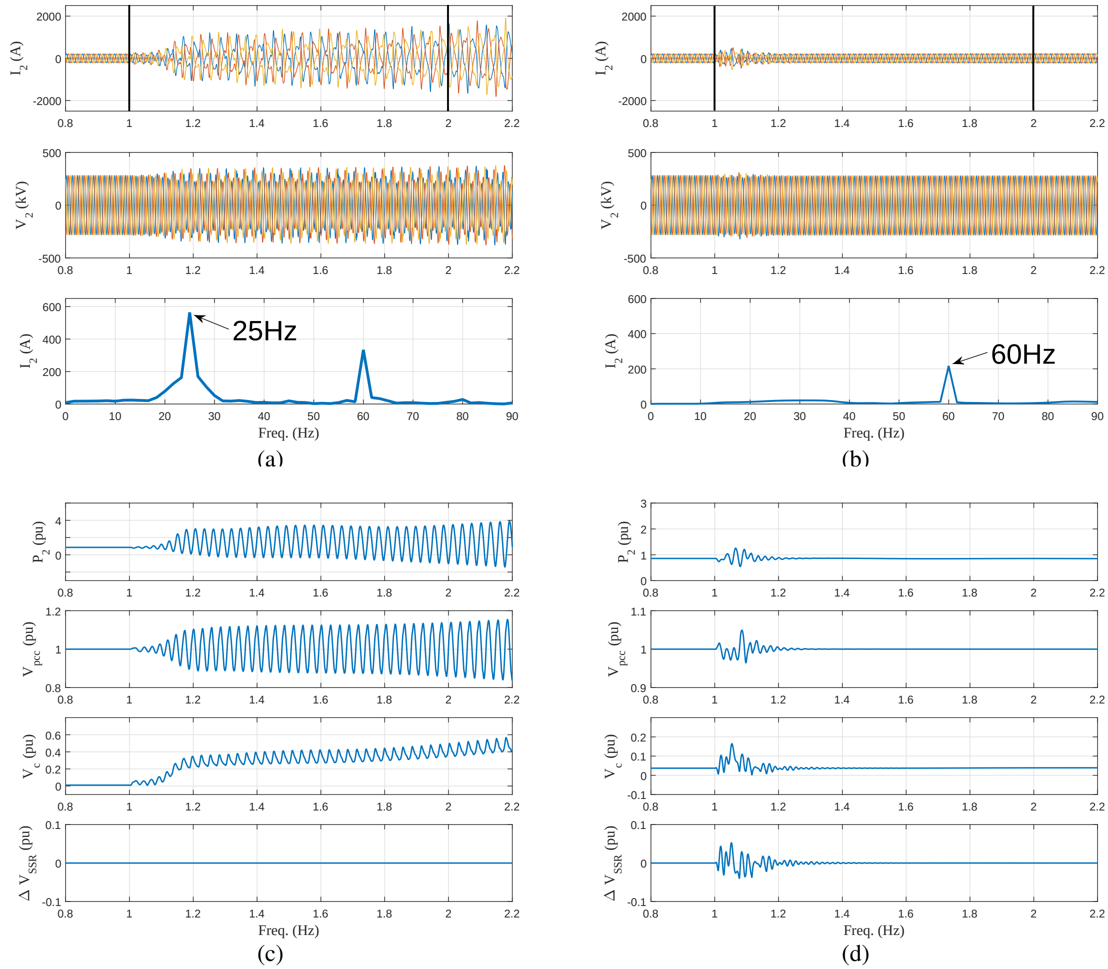

Fig. 14: Event 1. Without SSR control: (14a) and (14c); with SSR control: (14b) and (14d).

To test its performance under different conditions, the SSR control was tested for Event 3 with the same gain $K_{Vc} = 0.8$. Compared to WF2's power output in Event 1 (less than 1 pu), Event 3 had a higher wind power from WF2 (2 pu) due to faster wind speed. Fig. 15 gives the comparison of without and with SSR control for Event 3. It can be seen that the SSR mitigation control can provide damping to SSR oscillation and make the system more stable.

We also re-tested the SSR control under Event 1 with 300 online wind turbines in WF2. The testbed simulation results again show SSR control can effectively mitigate SSR.

VI. Conclusion

In this paper, a testbed is built in Matlab/Simpowersystems to replicate three real-world wind farm SSR events. The challenges of testbed building are (i) how to assume a simplified yet adequate system topology, and (ii) how to configure the testbed with very limited known information on the events. We rely on public transmission grid information to configure the transmission system parameters and rely on type-3 wind SSR characteristics to tune wind farm parameters. The developed testbed can successfully replicate the real-world events. Impact of online wind turbine number, wind speed are examined using the testbed. Finally, an SSR mitigation strategy relying on GSC supplementary control is implemented in the testbed and its effectiveness is confirmed.

Appendix

TABLE III: Parameters of one DFIG wind turbine

Parameter	Value (SI)	Per-unit (pu)
Rated power	1.5 MW	0.9
DC-link voltage	1150 V	
Rated voltage	575 V	1
Nominal freq.	60 Hz	1
Wind speed at Pmax	11 m/s	
$L_{ls}(X_{ls}), R_s$	94.5 μH, 5.6 mΩ	0.18, 0.023
$L'_{lr}(X'_{lr}), R'_r$	84.0 μH, 3.9 mΩ	0.16, 0.016
$L_m(X_m)$	1.5 mH	2.9
Inertial, poles	8.03 J, 6	
Friction factor	0.01	
C_{dc}	10 mF	
$L_c(X_{Lc}), R_c$	0.16 mH, 0.59 mΩ	0.3, 0.03
$C_1(B_1)$	2.9 mF	0.267
Current control (GSC)		$K_{pig} = 0.83$, $K_{iig} = 5$
DC-link control		$K_{pdc} = 8$, $K_{idc} = 400$
V_{ac} control		$K_{pac} = 8$, $K_{iac} = 400$
Current control (RSC)		$K_{pir} = 0.6$, $K_{iir} = 8$
Q control		$K_{pq} = 0.4$, $K_{iq} = 40$
PLL		$K_{p\mathrm{PLL}} = 60$
		$K_{i\mathrm{PLL}} = 1400$

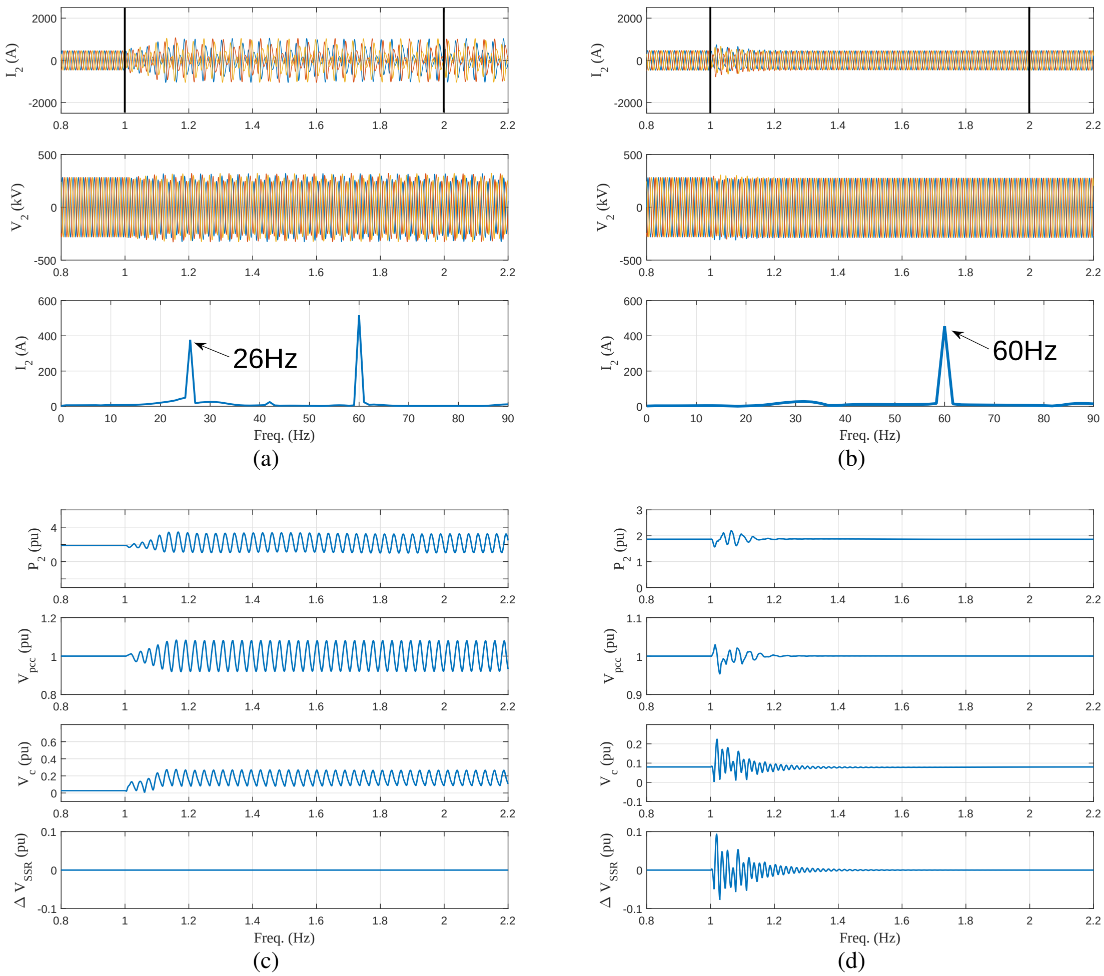

Fig. 15: Event 3. Without SSR control: (15a) and (15c); with SSR control: (15b) and (15d).

REFERENCES

[1] L. Fan, R. Kavasseri, Z. L. Miao, and C. Zhu, "Modeling of DFIG-Based Wind Farms for SSR Analysis," *IEEE Transactions on Power Delivery*, vol. 25, no. 4, pp. 2073–2082, Oct 2010.

[2] X. Xie, X. Zhang, H. Liu, H. Liu, Y. Li, and C. Zhang, "Characteristic analysis of subsynchronous resonance in practical wind farms connected to series-compensated transmissions," *IEEE Transactions on Energy Conversion*, vol. 32, no. 8, pp. 1117–1126, Sept 2017.

[3] Y. Cheng, S. Huang, J. Rose, V. Pappu, and J. Conto, "Subsynchronous resonance assessment for a large system with multiple series compensated transmission circuits," *IET Renewable Power Generation*, no. 3, Aug 2018.

[4] S. H. Huang and G. Yanfeng, *South Texas SSR*. ERCOT ROS Meeting, May, 2018.

[5] L. Fan and Z. Miao, "Mitigating ssr using dfig-based wind generation," *IEEE Transactions on Sustainable Energy*, vol. 3, no. 3, pp. 349–358, July 2012.

[6] J. Adams, V. A. Pappu, and A. Dixit, "ERCOT experience screening for Sub-Synchronous Control Interaction in the vicinity of series capacitor banks," in *2012 IEEE Power and Energy Society General Meeting*, July 2012, pp. 1–5.

[7] G. D. Irwin, A. K. Jindal, and A. L. Isaacs, "Sub-synchronous control interactions between type 3 wind turbines and series compensated ac transmission systems," in *2011 IEEE Power and Energy Society General Meeting*, July 2011, pp. 1–6.

[8] M. Sahni, B. Badrzadeh, D. Muthumuni, Y. Cheng, H. Yin, S. . Huang, and Y. Zhou, "Sub-synchronous interaction in wind power plants- part ii: An ERCOT case study," in *2012 IEEE Power and Energy Society General Meeting*, July 2012, pp. 1–9.

[9] M. Sahni, D. Muthumuni, B. Badrzadeh, A. Gole, and A. Kulkarni, "Advanced screening techniques for sub-synchronous interaction in wind farms," in *IEEE PES T&D 2012*, May 2012, pp. 1–9.

[10] N. Karnik, D. Novosad, H. K. Nia, M. Sahni, M. Ghavami, and H. Yin, "An evaluation of critical impact factors for ssci analysis for wind power plants: A utility perspective," in *2017 IEEE Power Energy Society General Meeting*, July 2017, pp. 1–5.

[11] Y. Cheng, M. Sahni, D. Muthumuni, and B. Badrzadeh, "Reactance scan crossover-based approach for investigating ssci concerns for dfig-based wind turbines," *IEEE Transactions on Power Delivery*, vol. 28, no. 2, pp. 742–751, April 2013.

[12] R. K. Varma, S. Auddy, and Y. Semsedini, "Mitigation of subsynchronous resonance in a series-compensated wind farm using FACTS controllers," *IEEE Transactions on Power Delivery*, vol. 23, no. 3, pp. 1645–1654, July 2008.

[13] M. S. El-Moursi, B. Bak-Jensen, and M. H. Abdel-Rahman, "Novel statcom controller for mitigating ssr and damping power system oscillations in a series compensated wind park," *IEEE Transactions on Power Electronics*, vol. 25, no. 2, pp. 429–441, Feb 2010.

[14] A. E. Leon and J. A. Solsona, "Sub-synchronous interaction damping control for dfig wind turbines," *IEEE Transactions on Power Systems*, vol. 30, no. 1, pp. 419–428, 2015.

[15] *Rio Grande Valley Projects*. Electric Transmission Texas, 2016.

[16] *New ETT 345-kV lines begin delivering power to LRGV*. Electric Transmission Texas, 2016.

[17] B. Cassell, *250-MW Hidalo Wind project in Texas due for commercial ops on Sept 23*. GenerationHub.com, 2016.

[18] N. W. Miller, J. J. Sanchez-Gasca, W. W. Price, and R. W. Delmerico, "Dynamic modeling of ge 1.5 and 3.6 mw wind turbine-generators for stability simulations," in *2003 IEEE Power Engineering Society General Meeting (IEEE Cat. No.03CH37491)*, vol. 3, July 2003, pp. 1977–1983 Vol. 3.

[19] L. Fan and Z. Miao, "Type-3 Wind Analytical Model for SSR: Revisited," *USF Technical Report*, 2018.

Yin Li (S'13) received the B.S. degree in electrical engineering from University of South Florida (USF) in May 2014 and joined the USF Smart Grid Power Systems Lab in Aug. 2014 for Ph.D. study. He works on converter penetrated system modeling and control.

Lingling Fan (SM'08) received the B.S. and M.S. degrees in electrical engineering from Southeast University, Nanjing, China, in 1994 and 1997, respectively, and the Ph.D. degree in electrical engineering from West Virginia University, Morgantown, in 2001. Currently, she is an Associate Professor with the University of South Florida, Tampa, where she has been since 2009. She was a Senior Engineer in the Transmission Asset Management Department, Midwest ISO, St. Paul, MN, form 2001 to 2007, and an Assistant Professor with North Dakota State University, Fargo, from 2007 to 2009. Her research interests include power systems and power electronics. Dr. Fan serves an editor for IEEE Trans. Sustainable Energy and IEEE Trans. Energy Conversion.

Zhixin Miao (SM'09) received the B.S.E.E. degree from the Huazhong University of Science and Technology,Wuhan, China, in 1992, the M.S.E.E. degree from the Graduate School, Nanjing Automation Research Institute (Nanjing, China) in 1997, and the Ph.D. degree in electrical engineering from West Virginia University, Morgantown, in 2002.

Currently, he is with the University of South Florida (USF), Tampa. Prior to joining USF in 2009, he was with the Transmission Asset Management Department with Midwest ISO, St. Paul, MN, from 2002 to 2009. His research interests include power system stability, microgrid, and renewable energy.